Crystal chemistry, X-ray diffraction reference patterns, and bandgap studies for $(Ba_xSr_{1-x})_2CoWO_6$ ($x = 0.1$, 0.2, 0.3, 0.5, 0.7, and 0.9)

W. Wong-Ng,[1] G. Y. Liu,[2,a)] D. D. Shi,[2] Y. Q. Yang,[3] R. Derbeshi,[1] D. Windover,[1] and J. A. Kaduk[4]
[1]*National Institute of Standards and Technology, Materials Measurement Science Division, Gaithersburg, Maryland 20899, USA*
[2]*State Key Laboratory of Geological Processes and Mineral Resources, and Institute of Earth Sciences, China University of Geosciences, Beijing 100083, China*
[3]*Institute of Materials Science and Engineering, Sichuan University of Science and Engineering, Zigong 643000, China*
[4]*Illinois Institute of Technology, Department of Chemistry and Biochemistry, Chicago, Illinois 60616, USA*

(Received 22 April 2020; accepted 26 May 2020)

X-ray reference powder patterns and structures have been determined for a series of cobalt- and tungsten-containing cubic alkaline-earth perovskites, $(Ba_xSr_{1-x})_2CoWO_6$ ($x = 0.1$, 0.2, 0.3, 0.5, 0.7, and 0.9). The structure of the end members of the series, Sr_2CoWO_6 and Ba_2CoWO_6, were tetragonal and cubic, respectively, agreeing with the literature data. From Rietveld refinements, it was found that when $x = 0.1$ and 0.2, the structure was tetragonal $I4/m$ ($a = 5.60481(6)$ and $5.62305(11)$ Å and $c = 7.97989(12)$ and $7.9847(2)$ Å, respectively; $Z = 2$). When $x > 0.2$, the structure was cubic ($Fm\bar{3}m$, No. 225; $Z = 4$) (from $x = 0.3$ to 0.9, a increases from 7.98399(13) to 8.08871(10) Å). This tetragonal series of compounds exhibit the characteristics of a distorted double-perovskite structure. The bond valence sum values for the alkaline-earth (Ba, Sr) sites in all $(Ba_xSr_{1-x})_2CoWO_6$ members are greater than the ideal value of 2.0, indicating over-bonding situation, whereas for the W sites, as x increases, a change from under-bonding to slightly over-bonding situation was observed. Density functional theory calculations revealed that while Sr_2CoWO_6 is a semiconductor, Ba_2CoWO_6 and $SrBaCoWO_6$ are half-metals. Powder X-ray diffraction patterns of this series of compounds $(Ba_xSr_{1-x})_2CoWO_6$, with $x = 0.1$, 0.2, 0.3, 0.5, 0.7, and 0.9, have been submitted to be included in the Powder Diffraction File. © *2020 International Centre for Diffraction Data*.
[doi:10.1017/S0885715620000342]

Key words: $(Ba_xSr_{1-x})_2CoWO_6$, crystal structure, powder X-ray diffraction patterns, semiconductor, half-metals

I. INTRODUCTION

Double-perovskite transition-metal oxides (TMO), with a general formula $A_2BB'O_6$, have attracted increasing attention in recent years. These perovskites possess interesting structural and transport properties (e.g., magnetic, optical, and electrical) and exhibit a variety of exotic properties, including colossal magnetoresistance, high-temperature superconductivity, half-metallicity (differentiated conducting response of the spin-up and spin-down electrons), leading to possible applications in spintronic devices. As these materials are stable at high temperature, and a number of these materials show reasonably high values of power factors P [$P = S^2 \cdot \sigma$, where S is the Seebeck coefficient and σ is the electrical conductivity (Tritt, 1996)]; therefore, in recent years, they are also potential candidates for energy conversion applications.

In general, perovskites are distinguished by their ability to simultaneously accommodate a wide range of species on both the 12-fold coordinated A cation site and sixfold B cation sites. A mismatch between ionic sizes and radii for cations sharing the same crystallographic sites provides a driving force for the ordering of these structures. Complex perovskite oxides result from the ordering of B and B' cations in the octahedral sites of the primitive perovskite. Common examples of ordered arrangements for the B cations correspond to the general stoichiometries $A_2BB'O_6$ and $A_3B_2B'O_9$, which have been studied extensively (Viola *et al.*, 2003; Manoun *et al.*, 2013). Cobalt tungstate, with a general formula A_2CoWO_6 (A = Ba, Sr, and Ca) are among the largely studied double perovskites. The crystal field effect on the effective magnetic moment of these A_2CoWO_6 phases has been investigated by Lòpez *et al.* (2012).

The double-perovskite Sr_2CoWO_6 was first studied in the 1960s (Blasse, 1965; Galasso, 1969), and it was reported to be an antiferromagnet with $T_N = 22$ K (Blasse, 1965). The structure of $SrCoWO_6$ was described as having tetragonal distortion and it assumes a random distribution of Co and W atoms in the $I4/m$ space group (Kupriyanov and Fesenko, 1962; Viola *et al.*, 2003) with $a = 5.58277(1)$ Å and $c = 7.97740(1)$ Å. The double-perovskite Ba_2CoWO_6, on the other hand, is cubic, space group $Fm\bar{3}m$ (No. 225), with the lattice parameter, $a = 8.103$ Å (Cox *et al.*, 1967). It would be instructional to study the solid solution series of $(Ba_xSr_{1-x})_2CoWO_6$, to confirm where phase transition takes place across the series (Fresia *et al.*, 1959; Gateshki *et al.*, 2003; Zhao *et al.*, 2005; Manoun *et al.*, 2013), and to compute the electronic properties including the bandgap value of the selected solid solution member.

a)Author to whom correspondence should be addressed. Electronic mail: guangyaoliu@hotmail.com

There are two main goals in the current study. First, the structures of $(Ba_xSr_{1-x})_2CoWO_6$ ($x = 0.1$, 0.2, 0.3, 0.5, 0.7, and 0.9) compounds are investigated for the effects of ionic size difference between Ba^{2+} and Sr^{2+} on their structure. We will also use density functional theory (DFT) to compute the electronic structure and the bandgap of the two end members and the intermediate member of this series ($x = 0$, 0.5, and 1). Additionally, the reference X-ray diffraction (XRD) patterns for $(Ba_xSr_{1-x})_2CoWO_6$ ($x = 0.2$ and 0.7) are measured to make them available as references through submission to the Powder Diffraction File (PDF, 2019).

II. EXPERIMENTAL

A. Materials synthesis

The $(Ba_xSr_{1-x})_2CoWO_6$ ($x = 0.1$–0.9) samples were prepared from stoichiometric amounts of $SrCO_3$, $BaCO_3$, Co_3O_4, and WO_3 using solid-state high-temperature techniques. The starting materials were mixed, pelletized, and heat-treated in air at 800 °C for 12 h and at 1000 °C for 12 h, with intermediate re-grindings, and finally at 1300 °C for 24 h. During each heat treatment, the samples were furnace cooled. The heat-treatment process was repeated until no further changes were detected in the powder XRD patterns.

B. Estimation of composition using X-ray fluorescence

The composition estimation of a sample of nominal $(Ba_{0.2}Sr_{0.8})_2CoWO_6$ was performed on a Bruker M4 Tornado micro X-ray fluorescence instrument. (The purpose of identifying the equipment in this article is to specify the experimental procedure. Such an identification does not imply recommendation or endorsement by the National Institute of Standards and Technology.) An Rh X-ray source, set to 50 kV and 300 μA, with a 20 μm monocapillary was used for excitation (S.N. 2001495). A Bruker XFlash 450 μm thick, Silicon Drift Detector (S.N. 11881_0239) was used for data collection for the scans. Each spectrum used a minimum peak sum of over 100 000 X-ray counts per analyzed element, reducing counting statistics as a source of uncertainty below all other contributions. Analyses were performed using Bruker Quantify version 1.6.0.286 with a standard Spectrum Elements method and calibrated for our instrument (S.N. 6099). For statistical sampling, 26 independent, 120 s live time measurements were performed, and the variance of the composition derived from these measurements was used for error analysis.

C. X-ray Rietveld refinements and powder reference patterns

The $(Ba_xSr_{1-x})_2CoWO_6$ ($x = 0.1$, 0.2, 0.3, 0.5, 0.7, and 0.9) samples were mounted as acetone slurries on a zero-background single-crystal Si sample holder. The X-ray powder patterns of the former samples were measured on a Bruker "stock" D2 Phaser diffractometer with 141 mm radius, Cu tube, 0.6 mm divergence slit, 2.5° Soller slits, a LynxEye position-sensitive detector, with a Ni filter. The Cu$K\alpha_{1/2}$ wavelengths were 1.5405929/1.544451 Å. (Operation condition: 30 kV, 10 mA, 5–130° 2θ in 0.0202144° steps, 0.5 s step^{-1}).

The Rietveld refinement technique (Rietveld, 1969) with software suite GSAS (Larson and von Dreele, 2004) was used to determine the structure. Reference patterns were obtained with a Rietveld pattern decomposition technique. Using this technique, the reported peak positions were derived from the extracted integrated intensities, and positions were calculated from the lattice parameters. When peaks are not resolved at the resolution function, the intensities are summed, and an intensity-weighted d-spacing is reported.

D. Bond valence sum calculations

The bond valence sum (BVS) values for the Ba, Sr, Co, and W sites in $(Ba_xSr_{1-x})_2CoWO_6$ were calculated using the Brown–Altermatt empirical expression (Brown and Altermatt, 1985; Brese and O'Keeffe, 1991). The BVS of an atom i is defined as the sum of the bond valences v_{ij} of all the bonds from atoms i to atoms j. The most commonly adopted empirical expression for the bond valence v_{ij} as a function of the interatomic distance d_{ij} is $v_{ij} = \exp[(R_0 - d_{ij})/B]$. The parameter, B, is commonly taken to be a "universal" constant equal to 0.37 Å. The values for the reference distance R_0 for Ba^{2+}–O, Sr^{2+}–O, W^{6+}–O, Co^{2+}–O are 2.29, 2.118, 1.921, and 1.692, respectively (Brown and Altermatt, 1985; Brese and O'Keeffe, 1991). If more than one atom type occupies the same site, the resulting BVS is the weighted sum of each site occupancy.

E. Bandgap calculations

We used the linearized augmented planewave (LAPW) method for the computation of the electronic structure within DFT. The calculations were performed using the ELK package (2018). The generalized gradient approximations (GGA) of Perdew, Burke, and Ernzerhof were used for the correlation and exchange potentials (Perdew *et al.*, 1996). The atomic radii are 2.5 a.u. for Ba, 2.24 a.u. for Sr, 2.01 a.u. for Co, 1.82 a.u. for W, and 1.57 a.u. for O, respectively. The RK_{max} parameter is set to be 7. Self-interaction correction for d electrons are introduced by an on-site Coulomb and exchange interactions, namely the Hubbard and exchange parameter U and J, with $U = 0.329$ and $J = 0.061$ Ry for Co and $U = 0.193$ and $J = 0.035$ Ry for W (Solovyev *et al.*, 1994). The energy convergence criteria are 10^{-5} Ry and the charge convergence criteria are 10^{-3}.

III. RESULTS AND DISCUSSION

The atomic ratio for Ba/Co, Sr/Co, and W/Co for the nominal $(Ba_{0.2}Sr_{0.8})_2CoWO_6$ sample were calculated using the X-ray fluorescence technique, with the Co concentration normalized to 1. The results show that the ratio of concentration for Sr/Co = 1.75 ± 0.30 (XRD value of 1.6) and W/Co [0.99 ± 0.17] (XRD value of 1) agree with 95% confidence ($K = 1$ confidence interval) and that the ratio of the concentration of Ba/Co = 0.317 ± 0.054 (XRD value of 0.4) agrees with 68% confidence ($K = 2$ confidence interval). Note that the uncertainties stated within the brackets represent 1 sigma (s) estimates.

The results of Rietveld refinement for the $(Ba_xSr_{1-x})_2CoWO_6$ ($x = 0.1$–0.9) series are shown in Table I and Figures 1 and 2. Table I gives various refinement statistical

TABLE I. Rietveld refinement residuals for $(Ba_xSr_{1-x})_2CoWO_6$ ($x = 0.1$, 0.2, 0.3, 0.5, 0.7, and 0.9).

Composition	R_{wp}	R_p	χ^2
$(Ba_{0.1}Sr_{0.9})_2CoWO_6$ ($x = 0.1$)	0.0311	0.0241	1.42
$(Ba_{0.2}\ Sr_{0.8})_2CoWO_6$ ($x = 0.2$)	0.0716	0.0510	1.27
$(Ba_{0.3}Sr_{0.7})_2CoWO_6$ ($x = 0.3$)	0.0623	0.0478	1.19
$(Ba_{0.5}Sr_{0.5})_2CoWO_6$ ($x = 0.5$)	0.0687	0.0528	1.13
$(Ba_{0.7}Sr_{0.3})_2CoWO_6$ ($x = 0.7$)	0.0767	0.0653	1.18
$(Ba_{0.9}Sr_{0.1})_2CoWO_6$ ($x = 0.9$)	0.0894	0.0712	1.29

For $x = 0.1$ and 0.2, the structure is tetragonal $I4/m$, and for $x = 0.3$–0.9, the structure is cubic $Fm\bar{3}m$ (No. 225).

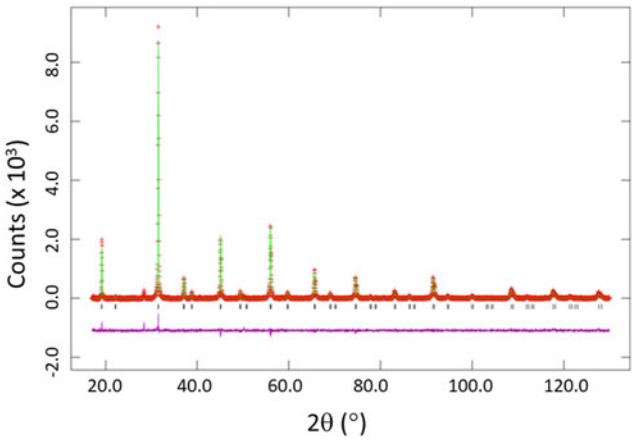

Figure 1. Observed (crosses), calculated (solid line), and difference XRD patterns (bottom) for $(Ba_{0.7}Sr_{0.3})_2CoWO_6$ by a Rietveld analysis technique. The difference pattern is plotted at the same scale as the other calculated peak positions. The small peak in the 2θ (°) around 28° region is the K_β peak of the 110 reflection. Its presence does not interfere with the refinement.

agreement factors, whereas in Figures 1 and 2, the observed (crosses), calculated (solid line), and difference XRD patterns (bottom) for $(Ba_xSr_{1-x})_2CoWO_6$ ($x = 0.7$ and 0.2) are illustrated; the difference pattern is plotted at the same scale. The row of tick marks indicates the calculated peak positions. In these figures, the small peak in the 2θ (°) around 28° region is the K_β peak of the 110 reflection. Its presence does not interfere with the refinement. Table II lists the lattice parameters, while atomic coordinates and displacement parameters are shown in Table III. The bond distances and BVS values are summarized in Table IV.

The $(Ba_xSr_{1-x})_2CO_6$ solid solution series is confirmed to be double perovskite, having two types of structures across the

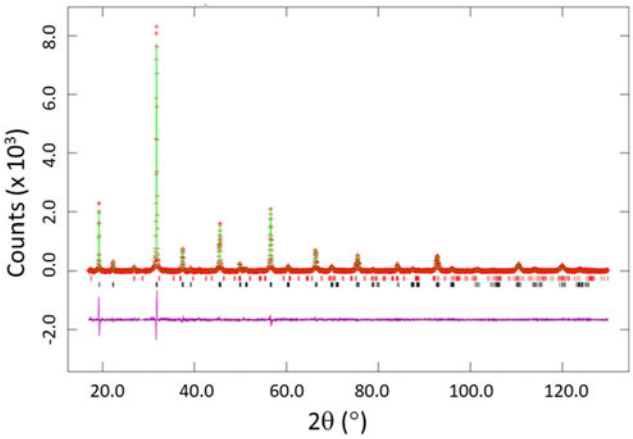

Figure 2. Observed (crosses), calculated (solid line), and difference XRD patterns (bottom) for $(Ba_{0.2}Sr_{0.8})_2CoWO_6$ by a Rietveld analysis technique. The difference pattern is plotted at the same scale as the other calculated peak positions.

series. When Sr concentration is rich ($x = 0.1$ and 0.2), the structure is of Sr_2CoWO_6 type, tetragonal $I4/m$ (No. 87) ($a = 5.60481(6)$ and $5.62305(11)$ Å and $c = 7.97989(12)$ and $7.9847(2)$ Å, respectively). These unit-cell parameters are related to a_0 (ideal cubic perovskite, $a_0 \approx 3.95$ Å) as $a \approx b \approx \sqrt{2}a_0$, $c \approx 2a_0$. When $x > 0.2$, the structure was found to be cubic $Fm\bar{3}m$ (No. 225) (from $x = 0.3$–0.9, a increases from 7.98399(13) to 8.08871(10) Å, respectively). These cubic unit-cell parameters are related to a_0 as $a \approx 2a_0$. In both type of structures, there is an apparent disorder in the Ba and Sr sites, in contrast to the ordering of CoO_6 and WO_6 octahedra. Figure 3 illustrates changes in the unit-cell volumes, V, in the $(Ba_xSr_{1-x})_2CoWO_6$ series ($x = 0.1$–0.9) as a function of x. V increases slightly (5.76%) across the entire solid solution series [from 500.360(14) to 529.22(2) Å^3].

Figures 4–6 illustrate the tetragonal structure of $(Ba_xSr_{1-x})_2CoWO_6$ viewing along the a-axis, ab-diagonal, and c-axis, respectively. The structure is built from corner-sharing WO_6 and CoO_6 octahedra just like the rock salt structure. In the tetragonal structure, it is obvious that there is a rotational mismatch of the distorted WO_6 and CoO_6 octahedra while viewing along the c-axis. This series of compounds exhibit the characteristics of the distorted double-perovskite structure, with the rotational mismatch angles of 13.776° counter-clockwise for CoO_6 octahedra, 12.143° clockwise for WO_6 octahedra in $x = 0.1$ compounds, and the rotational mismatch angles of 7.44° counter-clockwise for CoO_6

TABLE II. Cell parameters for $(Ba_xSr_{1-x})_2CoWO_6$ ($x = 0.1$, 0.2, 0.3, 0.4, 0.5, 0.6, 0.7, 0.8, and 0.9).

Chemical formula	a	c	V	d_{cal}	Z
$(Ba_{0.1}Sr_{0.9})_2CoWO_6$ ($x = 0.1$)	5.60481(6)	7.97989(12)	250.680(7)	6.942	2
			501.360		4
$(Ba_{0.2}Sr_{0.8})_2CoWO_6$ ($x = 0.2$)	5.62305(11)	7.9847(2)	252.466(13)	7.023	2
			504.932		4
$(Ba_{0.3}Sr_{0.7})_2CoWO_6$ ($x = 0.3$)	7.98399(13)		508.93(2)	7.098	4
$(Ba_{0.5}Sr_{0.5})_2CoWO_6$ ($x = 0.5$)	8.02004(11)		515.86(2)	7.259	4
$(Ba_{0.7}Sr_{0.3})_2CoWO_6$ ($x = 0.7$)	8.05447(10)		522.530(12)	7.419	4
$(Ba_{0.9}Sr_{0.1})_2CoWO_6$ ($x = 0.9$)	8.08871(10)		529.22(2)	7.574	4

For $x = 0.1$ and 0.2, the structure is tetragonal $I4/m$, and for $x = 0.3$–1.0, the structure is cubic $Fm\bar{3}m$ (No. 225), $Z = 4$. For comparison purpose (with the same Z value per unit cell), the unit-cell volumes for the tetragonal compounds are doubled.

TABLE III. Atomic coordinates and displacement parameters for compounds for $(Ba_xSr_{1-x})_2CoWO_6$ ($x = 0.1$, 0.2, 0.3, 0.5, 0.7, and 0.9).

Atom	x	y	z	Site Occ.	U_{iso}	Wyckoff symbol
(1) $(Ba_{0.1}Sr_{0.9})_2CoWO_6$	($x = 0.1$)					
Ba1/Sr2	0	½	¼	0.1/0.9	0.0173(5)	4d
Co3	0	0	½	1.0	0.0130(10)	2b
W4	½	½	½	1.0	0.0153(4)	2a
O5	0.1764	0.2910	0	1.0	0.0004(14)	8h
O6	0	0	0.2378	1.0	0.0004(14)	4e
(2) $(Ba_{0.2}Sr_{0.8})_2CoWO_6$	($x = 0.2$)					
Ba1/Sr2	0	½	¼	0.2/0.8	0.0107(9)	4d
Co3	0	0	½	1.0	0.0130(10)	2b
W4	½	½	½	1.0	0.007(2)	2a
O5	0.21065	0.27393	0	1.0	0.02	8h
O6	0	0	0.24404	1.0	0.02	4e
(3) $(Ba_{0.3}Sr_{0.7})_2CoWO_6$	($x = 0.3$)					
Ba1/Sr2	¼	¼	¼	0.3/0.7	0.0159(8)	8c
Co3	0	0	0	1.0	0.017(2)	4a
W4	½	½	½	1.0	0.0142(6)	4b
O5	0.2614(2)	0	0	1.0	0.027(2)	24e
(4) $(Ba_{0.5}Sr_{0.5})_2CoWO_6$	($x = 0.5$)					
Ba1/Sr2	¼	¼	¼	0.5/0.5	0.0135(9)	8c
Co3	0	0	0	1.0	0.017(2)	4a
W4	½	½	½	1.0	0.0127(7)	4b
O5	0.26139(14)	0	0	1.0	0.024(2)	24e
(5) $(Ba_{0.7}Sr_{0.3})_2CoWO_6$	($x = 0.7$)					
Ba1/Sr2	¼	¼	¼	0.7/0.3	0.0128(7)	8c
Co3	0	0	0	1.0	0.023(2)	4a
W4	½	½	½	1.0	0.0157(6)	4b
O5	0.26139(14)	0	0	1.0	0.026(2)	24e
(6) $(Ba_{0.9}Sr_{0.1})_2CoWO_6$	($x = 0.9$)					
Ba1/Sr2	¼	¼	¼	0.7/0.3	0.0161(7)	8c
Co3	0	0	0	1.0	0.018(2)	4a
W4	½	½	½	1.0	0.0155(6)	4b
O5	0.2614(2)	0	0	1.0	0.026(2)	24e

For $x = 0.1$ and 0.2, the structure is tetragonal $I4/m$, and for $x = 0.3$–0.9, the structure is cubic $Fm\bar{3}m$ (No. 225).

octahedra, 6.999° clockwise for WO_6 octahedra in $x = 0.2$ compounds. One also observes the distorted tetragonal channels that are tilted with respect to the a-axis. Ba atoms were found inside the channels. From Figures 4–6, it is seen that WO_6 and CoO_6 octahedra alternate with each other along the ab-diagonal or c-axis. Viewing along the [001] direction of the pseudo-cubic cell, the alternating CoO_6 and WO_6 octahedra were found to tilt in an antiphase fashion. Agreeing with Viola *et al.* (2003), this tilting corresponds to the $a^0a^0c^-$ Glazer's notation (1972) derived by Woodward (1997) for

TABLE IV. Bond distances and BVS values for $(Ba_xSr_{1-x})_2CoWO_6$ [$x = 0.1$ (T), 0.2 (T), 0.3 (C), 0.5 (C), 0.7 (C), and 0.9 (C)].

		Bond distances (Å) and BVS values							
Atom	Atom	(i) $x = 0.1$	BVS	(ii) $x = 0.2$	BVS				
(a) Tetragonal phases									
Ba1/Sr1	O5 × 4	3.15118(3)	2.368	3.00077(5)	2.170				
	O5 × 4	2.51587(3)		2.64643(5)					
	O6 × 4	2.80410(3)		2.81193(5)					
	Ave	2.82372		2.81971					
Co3	O5 × 4	2.15949(2)	1.808	2.06474(4)	2.234				
	O6 × 2	2.09254(3)		2.04377(6)					
W4	O5 × 4	1.90691(3)	6.287	1.94312(4)	5.624				
	O6 × 2	1.89740(3)		1.94858(6)					
		(iii) $x = 0.3$	BVS	(iv) $x = 0.5$	BVS	(v) $x = 0.7$	BVS	(vi) $x = 0.9$	BVS
(b) Cubic phases									
Ba1/Sr1	O5 × 12	2.82424(5)	2.095	2.83698(5)	2.228	2.84916(5)	2.352	2.86128(5)	2.467
Co3	O5 × 6	2.0871(12)	2.063	2.0964(11)	2.011	2.1054(12)	1.963	2.1145(13)	1.915
W4	O5 × 6	1.9049(12)	6.267	1.9137(11)	6.120	1.9219(12)	5.985	1.9299(13)	5.857

The ideal BVS values are 2.0 for Ba1 site, 6.0 for the W site, and 2.0 for the Co site, respectively. The values for the reference distance R_0 for Ba^{2+}–O, Sr^{2+}–O, Co^{2+}–O, and W^{6+}–O are 2.29, 2.118, 1.692, and 1.921, respectively (Brown and Altermatt, 1985; Brese and O'Keeffe, 1991).

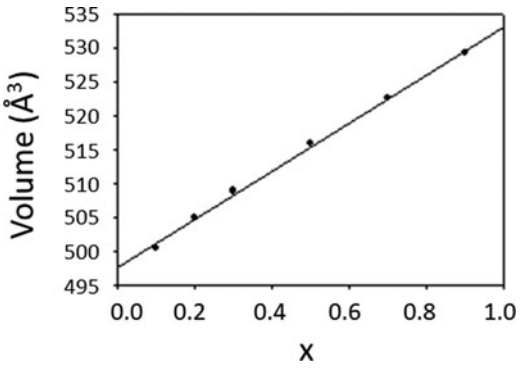

Figure 3. Compositional dependence of the unit-cell volume, *V*, for $(Ba_xSr_{1-x})_2CoWO_6$. For comparison purpose (with the same *Z* value per unit cell), the unit-cell volumes for the tetragonal compounds are doubled. A monotonic increase of *V* is observed as a function of *x*.

the 1:1 ordering of double perovskites (consistent with the space group *I*4/*m*). The distorted nature of the WO_6 and CoO_6 octahedra are also revealed in the bond distances of W–O and Co–O, while the bond angles of O–W–O and O–Co–O are either 90° or 180°. For example, the W–O distances range from 1.89740(3) to 1.94858(6) Å in WO_6 and from 2.15949(2) to 2.04377(6) Å in CoO_6. In Figure 7, the structure of cubic $(Ba_xSr_{1-x})_2CoWO_6$ is shown. Similar to the tetragonal structure, one finds alternate arrangement of the WO_6 and CoO_6 octahedra along all three-axis.

The Ba/Sr atoms were found to be inside the channels, occupying a 12 oxygen coordination site. The average Ba/Sr–O bond distances range from 2.51589(3) to 2.86128(5) Å. The BVS values of the (Ba, Sr) site are, in general, greater than the ideal value of 2.0. It is interesting that in the tetragonal case, the BVS value decreases from 2.368 to 2.170, but the opposite trend exists in the cubic case, increases from 2.095 to 2.467 when *x* increases from 0.3 to 0.9, respectively. All these values are greater than the ideal value of 2.0, indicating overbonding situation, or the cage size is too small.

The BVS values for the sixfold coordinated W site in both the tetragonal and cubic cases have deviated from the ideal value of 6.0. In both cases, as the concentration of Ba

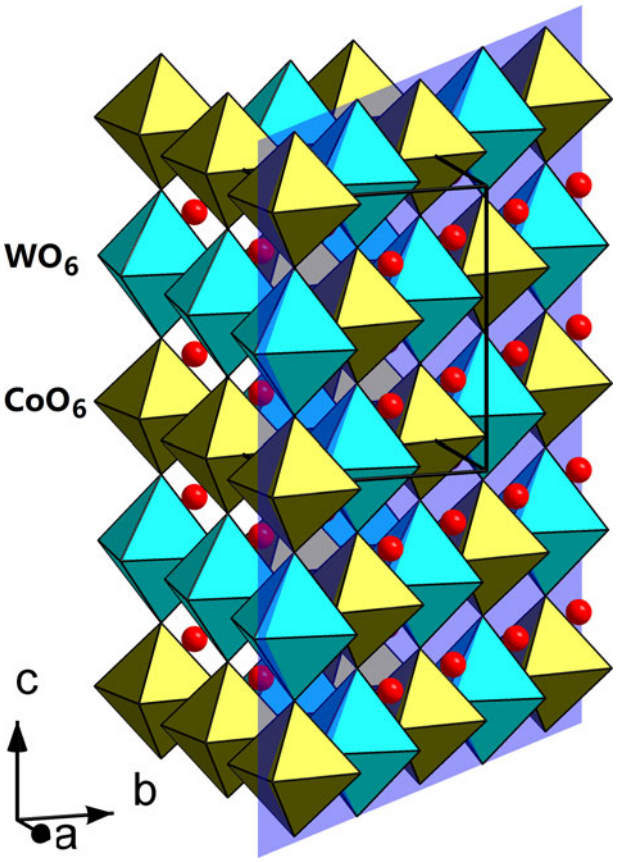

Figure 5. Tetragonal structure of $(Ba_{0.2}Sr_{0.8})_2CoWO_6$ along the *ab*-diagonal.

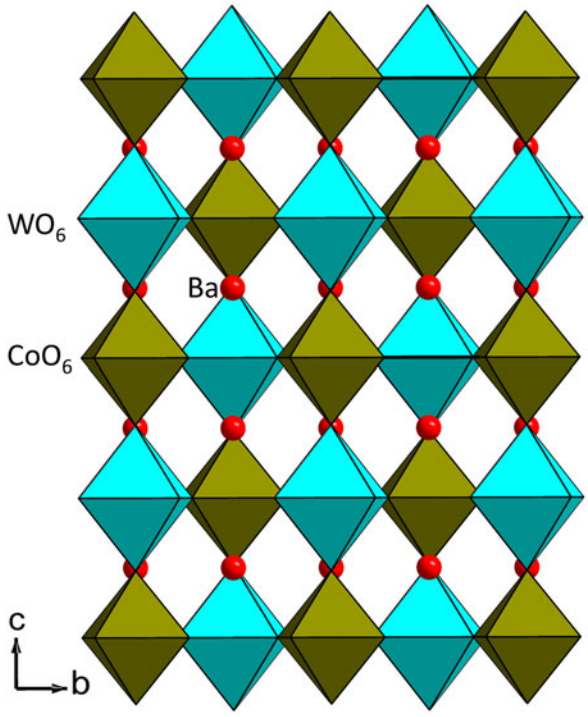

Figure 4. Tetragonal structure of $(Ba_{0.2}Sr_{0.8})_2CoWO_6$ viewed along the *a*-axis.

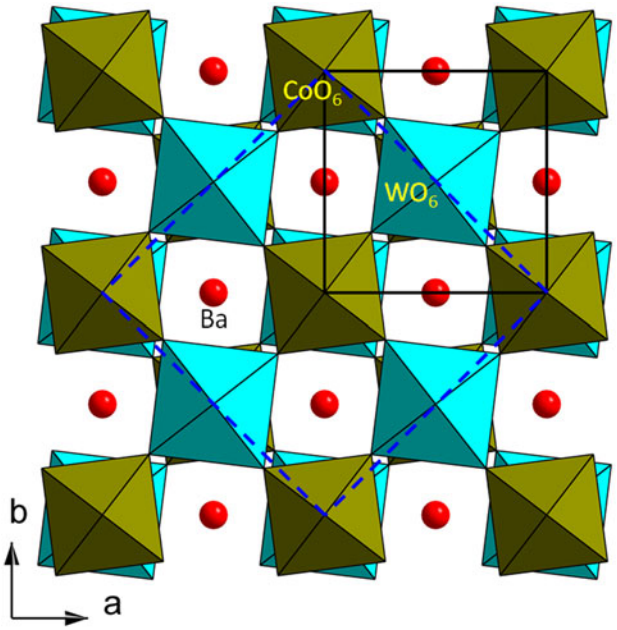

Figure 6. Tetragonal structure of $(Ba_{0.2}Sr_{0.8})_2CoWO_6$ viewed along the *c*-diagonal.

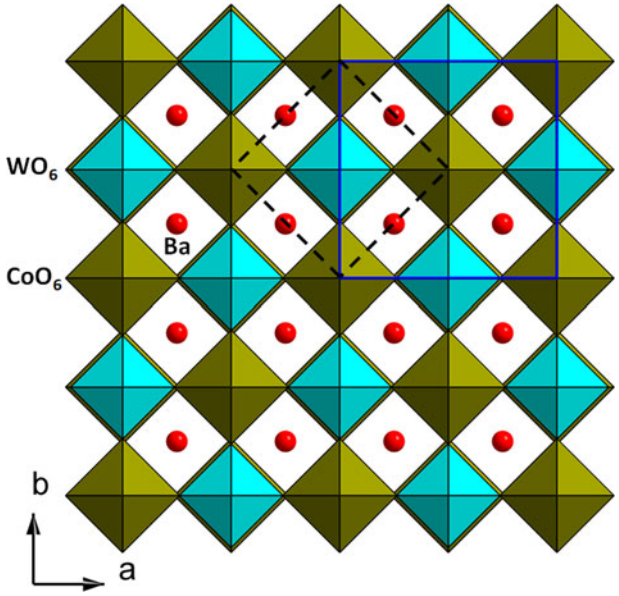

Figure 7. Cubic structure of $(Ba_{0.7}Sr_{0.3})_2CoWO_6$ viewed along the *a*-axis.

TABLE V. DFT calculated lattice constants and bandgap values (spin-up) using GGA and GGA + *U* methods.

	Lattice constants (Å)		Bandgap (eV)	
$(Ba_xSr_{1-x})_2CoWO_6$	*a*	*c*	GGA (spin-up/ spin-down)	GGA + *U* (spin-up/ spin-down)
$x = 0.0$	5.6416	8.1126	1.85/0.00	2.42/1.55
$x = 0.5$ (Tetragonal)	5.7224	8.0927	1.76/0.00	2.52/1.95
$x = 0.5$ (Cubic)	8.0090	–	1.68/0.00	2.57/0.00
$x = 1.0$	8.1583	–	1.92/0.00	2.71/0.00

increases, the BVS value decreases (from 6.287 to 5.624 Å in the tetragonal case and from 6.267 to 5.857 Å in the cubic case), indicating a change from over-bonding to slightly under-bonding situation. For the sixfold Co sites, although no specific trend is observed, all BVS values are slightly deviate from the ideal value of 2.0.

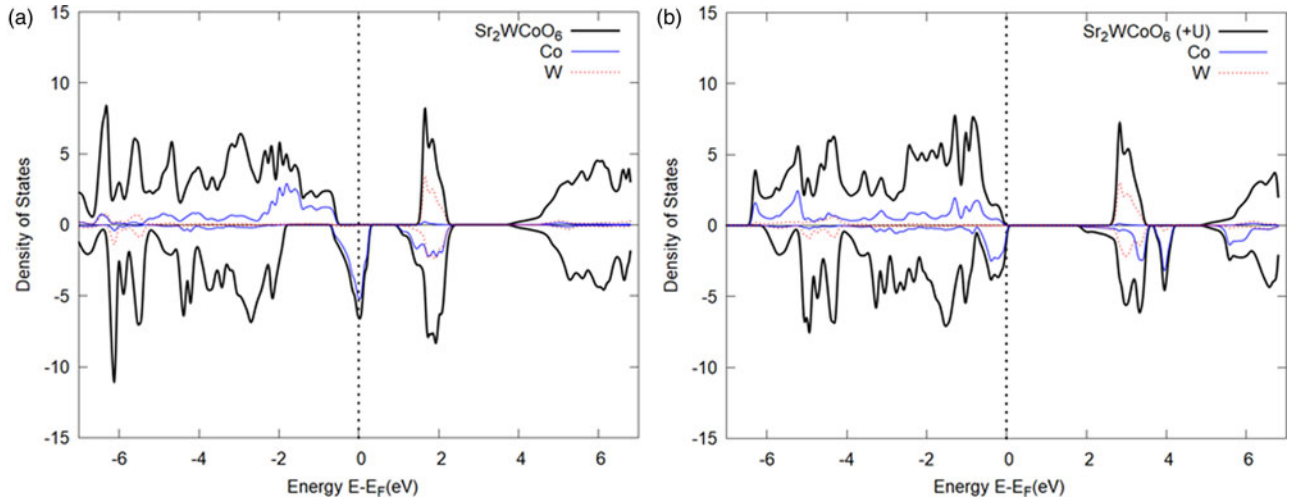

Figure 8. Bandgap calculations using DFT for Sr_2CoWO_6, (a) bandgap E_g using GGA and (b) using GGA + *U*. The partial DOS contribution from W and Co are shown.

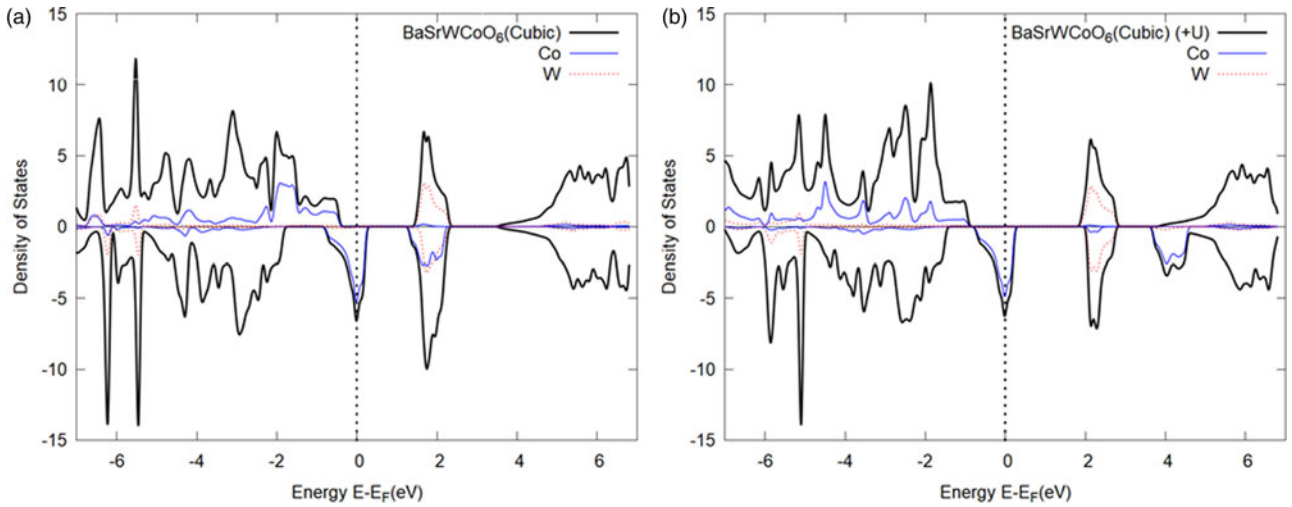

Figure 9. Bandgap calculations using DFT for $(SrBa)CoWO_6$ using a cubic model, (a) bandgap E_g using GGA and (b) using GGA + *U*. The partial DOS contribution from W and Co are shown.

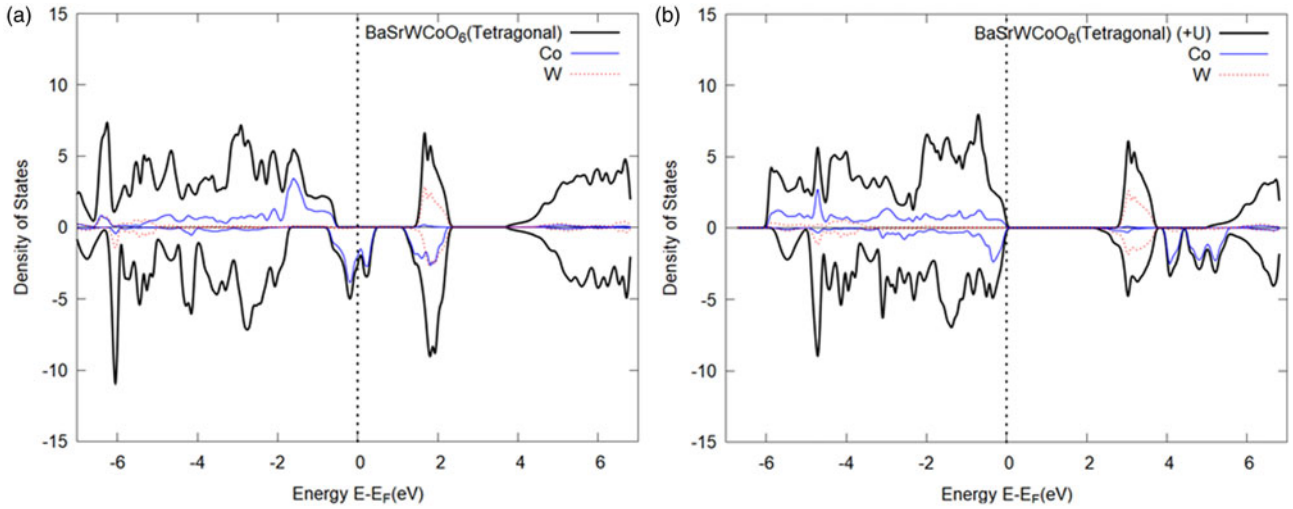

Figure 10. Bandgap calculations using DFT for (SrBa)$CoWO_6$ using a tetragonal model, (a) bandgap E_g using GGA and (b) using GGA + U. The partial DOS contribution from W and Co are shown.

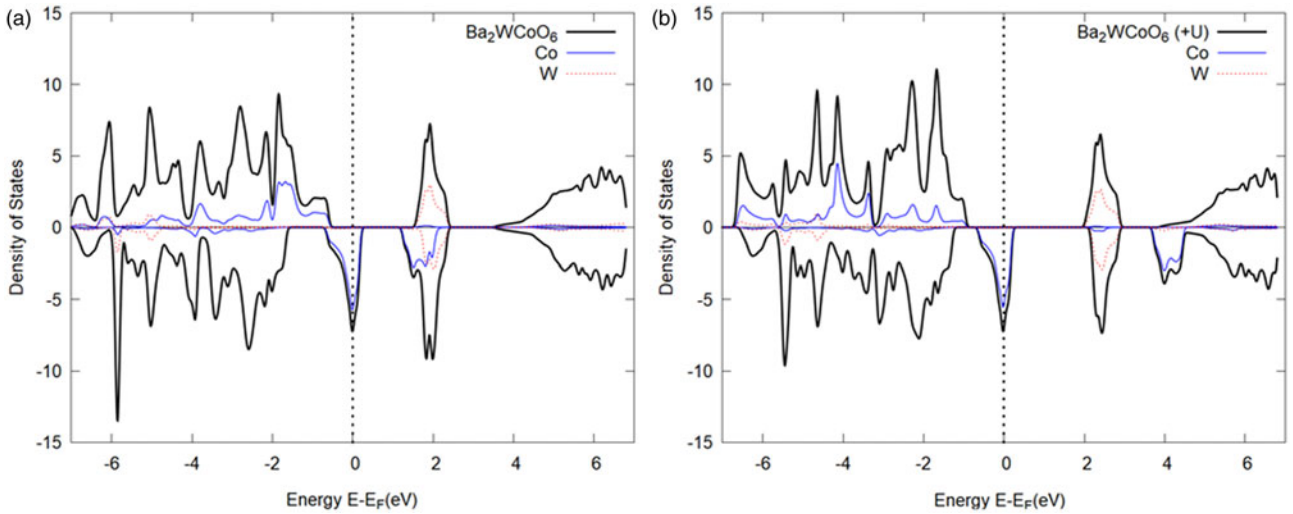

Figure 11. Bandgap calculations using DFT for Ba_2CoWO_6, (a) bandgap E_g using GGA and (b) using GGA + U. The partial DOS contribution from W and Co are shown.

TABLE VI. Magnetic moment (μ_B) of the $(Ba_xSr_{1-x})_2CoWO_6$ compounds. The interstitial presents the moment of interstitial electrons between atomic spheres.

	$x = 0.0$ (Sr_2CoWO_6)	$x = 0.5$ ($BaSrCoWO_6$)		$x = 1.0$ (Ba_2CoWO_6)
	Tetragonal		Cubic	
Interstitial	0.09	0.17	−0.02	0.01
Sr	−0.00	−0.00	−0.00	–
Ba		−0.00	−0.00	−0.00
Co	2.70	2.72	2.71	2.69
W	0.02	0.02	−0.03	−0.02
O	0.03	0.03	0.06	0.05
Total/f.u.	3.00	3.00	3.00	3.00

A. Bandgap calculations

Table V gives the DFT calculated lattice constants and bandgap values (spin-up) using GGA and GGA + U methods. Results of DFT calculations show that after considering Coulomb exchange ($U = 0.392$ and $J = 0.061$ Ry for Co and $U = 0.193$ and $J = 0.035$ Ry for W), the bandgaps increased about 0.5–0.7 eV (Figures 8–11). The calculated bandgap values are 2.71, 2.57, 2.52, and 2.42 eV for Sr_2CoWO_6 [Figure 8(b)], cubic $SrBaCoWO_6$ [Figure 9(b)], tetragonal $SrBaCoWO_6$ [Figure 10(b)], and Ba_2CoWO_6 [Figure 11(b)], respectively. From the results of the density of states (DOS) calculations, the state density of Sr_2CoWO_6 ($x = 0.0$) near the Fermi energy level is shown to be both zero in the spin-up and spin-down bands, which is a pattern of a typical semiconductor [Figure 8(b)]. The spin-up band of Ba_2CoWO_6 ($x = 1.0$) [Figure 11(b)] is zero near the Fermi energy level, while the state density of the spin-down band has a peak through the Fermi energy level, showing typical half metallicity [Figure 11(b)]. In other words, a half-metal is any substance that acts as a conductor to electrons of one spin orientation, but as an insulator or semiconductor to those of the opposite orientation. When $BaSrCoWO_6$ ($x = 0.5$) was calculated using the cubic structure model it is half-metallic [Figure 9(b)], while using the tetragonal structure model $BaSrCoWO_6$

TABLE VII. X-ray powder pattern for $(Ba_{0.2}Sr_{0.8})_2CoWO_6$, tetragonal $I4/m$ (No. 74) ($a = 5.62305(11)$ Å, $c = 7.9847(2)$ Å, $V = 252.466(13)$ Å^3, and $Z = 2$).

d_{cal}	I_{obs}	h	k	l		d_{cal}	I_{obs}	h	k	l	
4.5974	354	0	1	1		3.9825	53	0	0	2	M
3.9825	53	1	1	0	M	2.8173	999	1	1	2	
2.8115	560	0	2	0		2.4057	52	0	1	3	
2.3986	110	2	1	1	M	2.3986	110	1	2	1	M
2.2987	8	0	2	2		1.9962	165	0	0	4	
1.9881	298	2	2	0		1.8279	41	2	1	3	M
1.8279	41	1	2	3	M	1.8248	21	0	3	1	
1.7840	10	1	1	4		1.7788	12	2	2	2	+
1.6277	196	0	2	4		1.6243	363	3	1	2	M
1.6243	363	1	3	2	M	1.5362	18	0	1	5	
1.5325	12	0	3	3		1.5306	32	3	2	1	M
1.5306	32	2	3	1	M	1.4086	177	2	2	4	
1.4058	80	0	4	0		1.3481	19	2	1	5	M
1.3481	19	1	2	5	M	1.3456	18	3	2	3	M
1.3456	18	2	3	3	M	1.3443	19	1	4	1	M
1.3443	19	4	1	1	M	1.3278	6	1	3	4	M
1.3278	6	3	1	4	M	1.2620	74	1	1	6	
1.2576	139	3	3	2	+	1.2156	4	0	3	5	
1.2137	10	4	1	3	M	1.2137	10	1	4	3	M
1.1494	72	0	4	4		1.1179	5	0	1	7	
1.1158	13	2	3	5	M	1.1158	13	3	2	5	M
1.1136	16	0	5	1	+	1.0654	89	3	1	6	M
1.0654	89	1	3	6	M	1.0639	90	2	4	4	M
1.0639	90	4	2	4	M	1.0630	81	5	1	2	M
1.0630	81	1	5	2	M	1.0388	8	1	2	7	M
1.0388	8	2	1	7	M	1.0371	9	4	1	5	M
1.0371	9	1	4	5	M	1.0357	18	3	4	3	+
0.9981	9	0	0	8		0.9940	18	4	4	0	
0.9406	31	0	2	8		0.9391	32	3	3	6	
0.9374	90	3	5	2	+	0.9207	8	3	2	7	M
0.9207	8	2	3	7	M	0.9195	12	3	4	5	+
0.9183	9	1	6	1	M	0.9183	9	6	1	1	M
0.8920	51	2	2	8		0.8898	48	4	4	4	
0.8891	48	2	6	0	M	0.8891	48	6	2	0	M
0.8750	9	4	1	7	M	0.8750	9	1	4	7	M
0.8739	9	5	2	5	M	0.8739	9	2	5	5	M
0.8731	19	1	6	3	+						

The symbols "M" refers to peaks containing contributions from two reflections. The particular peak that has the strongest intensity in the entire pattern is assigned an intensity of 999 and other lines are scaled relative to this value. The d-spacing values are calculated values from refined lattice parameters, and "I" represents integrated intensity values.

TABLE VIII. X-ray powder pattern for $(Ba_{0.7}Sr_{0.3})_2CoWO_6$, cubic $Fm\bar{3}m$ (No. 225) ($Z = 4$, $a = 8.02004(11)$ Å, and $V = 515.86(2)$ Å^3).

d_{cal}	I_{obs}	h	k	l		d_{cal}	I_{obs}	h	k	l	
4.6502	165	1	1	1		4.0272	2	2	0	0	
2.8477	999	2	2	0		2.4285	81	3	1	1	
2.3251	20	2	2	2		2.0136	295	4	0	0	
1.8478	37	3	3	1		1.6441	394	4	2	2	
1.5501	47	3	3	3	M	1.5501	47	5	1	1	M
1.4238	186	4	4	0		1.3614	35	5	3	1	
1.2735	167	6	2	0		1.2283	12	5	3	3	
1.2143	4	6	2	2		1.1626	66	4	4	4	
1.1279	21	5	5	1	M	1.1279	21	7	1	1	M
1.0763	212	6	4	2		1.0486	25	5	5	3	M
1.0486	25	7	3	1	M	1.0068	29	8	0	0	
0.9840	4	7	3	3		0.9492	124	8	2	2	M
0.9492	124	6	6	0	M	0.9301	17	5	5	5	M
0.9301	17	7	5	1	M	0.9005	117	8	4	0	
0.8841	26	7	5	3	M	0.8841	26	9	1	1	M
0.8586	96	6	6	4							

The symbols "M" refers to peaks containing contributions from two reflections. The particular peak that has the strongest intensity in the entire pattern is assigned an intensity of 999 and other lines are scaled relative to this value. The d-spacing values are calculated values from refined lattice parameters, and "I" represents integrated intensity values.

($x = 0.5$) is a semiconductor [Figure 10(b)]. The total energy of the tetragonal structure is higher than that of the cubic structure when there is no Hubbard potential added to the d-electrons, but it changes to a lower energy value when the Hubbard potential is added, which illustrates that the Hubbard potential influences the stability of a structure and a reasonable U and J values should be used to match the experiments. It also seems to show that the Hubbard potential should have been included in the calculations from the beginning of the structure optimization process. The result of U and J addition is somewhat different from that of XRD. XRD gave better Rietveld refinement results for the cubic structure but calculation with the addition of Hubbard potential ($U = 0.392$ and $J = 0.061$ Ry for Co and $U = 0.193$ and $J = 0.035$ Ry for W) showed the tetragonal structure to be more stable. The DFT calculations used an ordered Ba and Sr model in the tetragonal case; however, we did not observe any satellite peaks related to the ordered feature in the XRD diffraction pattern, indicating a disordered structure. Lastly, in all cases, the state density near the Fermi energy level is almost completely contributed by the Co atom from its projection, and the magnetic moments of these compounds also almost come entirely from the Co atoms (Table VI).

B. Reference XRD pattern

Examples of reference patterns, namely the tetragonal $(Ba_{0.2}Sr_{0.8})_2CoWO_6$ and the cubic $(Ba_{0.7}Sr_{0.3})_2CoWO_6$, are given in Tables VII and VIII, respectively. In these patterns, the symbols "M" refers to peaks containing contributions from two reflections. The particular peak that has the strongest intensity in the entire pattern is assigned an intensity of 999 and other lines are scaled relative to this value. In general, the d-spacing values are calculated values from refined lattice parameters. The intensity values reported are integrated intensities (rather than peak heights) based on the corresponding profile parameters, as reported in Table I. For resolved overlapped peaks, intensity-weighted calculated d-spacing, along with the observed integrated intensity and the hkl indices of both peaks (for "M") are used. For peaks that are not resolved at the instrumental resolution, the intensity-weighted average d-spacing and the summed integrated intensity value are used. In the case of a cluster, unconstrained profile fits often reveal the presence of multiple peaks, even when they are closer than the instrumental resolution. In this situation, both d-spacing and intensity values are reported independently. The $(Ba_xSr_{1-x})_2CoWO_6$ ($x = 0.1$, 0.2, 0.3, 0.5, 0.7, and 0.9) patterns have been submitted for inclusion in the PDF.

IV. SUMMARY

Crystal structures and reference patterns of the $(Ba_xSr_{1-x})_2CoWO_6$ ($x = 0.1$, 0.2, 0.3, 0.5, 0.7, and 0.9) series of compounds have been determined and submitted to the PDF. $(Ba_xSr_{1-x})_2CoWO_6$ adopts a double-perovskite structure. From $x = 0$–0.2, the structure is tetragonal with space group $I4/m$, whereas when $x \geq 0.3$ the structure is cubic with

a space group of $Fm\bar{3}m$. The alternating CoO_6 and WO_6 octahedra were found to tilt in an antiphase fashion, corresponding to the $a^0a^0c^-$ Glazer's notation for the 1:1 ordering of double perovskites, consistent with the space group $I4/m$. All Ba sites have 12-fold coordination environment and all the ordered W and Co sites are sixfold (octahedral) coordinated. The BVS values for the Ba sites are all greater than the ideal value of 2.0 in both the tetragonal and cubic cases, indicating overbonding situation, or compressive coordination environment. DFT calculations concluded that with the addition of Hubbard potential on *d*-electrons the solid solution formation increases the bandgap width as compared to the end members, namely bandgap values of 2.43, 2.69, and 2.36 eV for Sr_2CoWO_6, $SrBaCoWO_6$, and Ba_2CoWO_6, respectively. Furthermore, while Sr_2CoWO_6 is a semiconductor, $SrBaCoWO_6$ and Ba_2CoWO_6 are half-metals.

SUPPLEMENTARY MATERIAL

The supplementary material for this article can be found at https://doi.org10.1017/S0885715620000342.

ACKNOWLEDGEMENT

ICDD is acknowledged for the Grants-in-Aid assistance for the project. Grant No. 0903, Grant holder James A. Kaduk.

Blasse, G. (**1965**). "Some magnetic properties of mixed metal oxides with ordered perovskite structure," Philips Res. Rep. **20**, 327.

Brese, N. E. and O'Keeffe, M. (**1991**). "Bond-valence parameters for solids," Acta Crystallogr. B **47**, 192–197.

Brown, I. D. and Altermatt, D. (**1985**). "Bond-valence parameters obtained from a systematic analysis of the inorganic crystal structure database," Acta Crystallogr. B **41**, 244–247.

Cox, D. E., Shirane, G., and Frazer, B. C. (**1967**). "Neutron-diffraction study of anti-ferromagnetic Ba_2CoWO_6 and Ba_2NiWO_6," J. Appl. Phys. **38**, 1459.

Elk package (**2018**). Elk, an all-electron full-potential linearised augmented-plane wave (LAPW) code with many advanced features. Written originally at Karl-Franzens-Universität Graz as a milestone of the EXCITING EU Research and Training Network. The code is freely available under the GNU General Public License (version 6.3.2, 2018).

Fresia, E. J., Katz, L., and Ward, R. (**1959**). "Cation substitution in perovskite-like phases," J. Am. Chem. Soc. **81**, 4783.

Galasso, F. (**1969**). *Structure, Properties and Preparation of Perovskite-Type Compounds* (Pergamon Press, Oxford).

Gateshki, M., Igartua, J. M., and Hernandez-Bocanegra, E. (**2003**). "X-ray powder diffraction results for the phase transitions in Sr_2MWO_6 (M = Ni, Zn, Co, Cu) double perovskite oxides," J. Phys. Condens. Matter. **15**, 6199.

Glazer, A. M. (**1972**). "The classification of tilted octahedra in perovskites," *Acta Crystallogr. B* **28**, 3384.

Kupriyanov, M. F. and Fesenko, E. G. (**1962**). "X-ray diffraction study of phase transitions in some perovskites," Kristallografiya **7**, 451–453.

Larson, A. C. and von Dreele, R. B. (**2004**). "General Structure Analysis System (GSAS)," Los Alamos National Laboratory Report LAUR 86-748, Los Alamos, USA.

Lòpez, C. A., Saleta, M. E., Curiale, J., and Sānchez, R. D. (**2012**). "Crystal field effect on the effective magnetic moment in A_2CoWO_6 (A= Ca, Sr and Ba)," Mater. Res. Bull. **47**, 1158–1163.

Manoun, B., Ezzahi, A., Benmokhtar, S., Bihc, L., Tamraoui, Y., Haloui, R., Mirinioui, F., Addakiri, S., Igartua, J. M., and Lazor, P. (**2013**). "X-ray diffraction and Raman spectroscopy studies of temperature and composition induced phase transitions in $Ba_{2-x}Sr_xMWO_6$ (M = Ni, Co and $0 \leqslant x \leqslant 2$) double perovskite oxides," J. Mol. Struct. **1045**, 1–14.

PDF (**2019**). Powder Diffraction File, produced by International Centre for Diffraction Data, 12 Campus Blvd., Newtown Squares, PA 19073-3273, USA.

Perdew, J., Burke, K., and Ernzerhof, M. (**1996**). "Generalized gradient approximation made simple," Phys. Rev. Lett. **77**, 3865.

Rietveld, H. M. (**1969**). "A profile refinement method for nuclear and magnetic structures," J. Appl. Cryst. **2**, 65–71.

Solovyev, I. V., Dederichs, P. H., and Anisimov, V. I. (**1994**). "Corrected atomic limit in the local-density approximation and the electronic structure of *d* impurities in Rb," Phys. Rev. B **50**, 16861.

Tritt, T. M. (**1996**). "Thermoelectrics run hot and cold," Science **272**, 1276–1277.

Viola, M. C., Martínez-Lope, M. J., Alonso, J. A., Martínez, J. L., De Paoli, J. M., Pagola, S., Pedregosa, J. C., Fernández-Díaz, M. T., and Carbonio, R. E. (**2003**). "Structure and magnetic properties of Sr_2CoWO_6: an ordered double perovskite containing Co^{2+}(HS) with unquenched orbital magnetic moment," Chem. Mater. **15**, 1655–1663.

Woodward, P. M. (**1997**). "Octahedral tilting in perovskites. I. Geometrical considerations," Acta Crystallogr. B **53**, 32–43.

Zhao, F., Yue, Z. X., Gui, Z. L., and Li, L. T. (**2005**). "Preparation, characterization and microwave dielectric properties of A_2BWO_6 (A = Sr, Ba; B = Co, Ni, Zn) double perovskite ceramics," Jpn. J. Appl. Phys. **44**, 8066.